A 25 MG MAGNETICALLY ACTUATED MICROROBOT WALKING AT > 5 BODY LENGTHS/SEC

Dana Vogtmann, Ryan St. Pierre, and Sarah Bergbreiter
The University of Maryland, College Park, MD, USA

ABSTRACT

This paper presents the first demonstration of an untethered legged microrobot walking at speeds greater than 5 body lengths/second. This work integrates contributions in multi-material robot leg design and microfabrication as well as high power actuation using an external magnetic field. The resulting 25 mg, 4 mm x 4 mm x 5 mm hexapedal robot has been measured walking at speeds in excess of 20 mm/sec, reaching a top speed of 25.5 mm/sec (6.4 body lengths/sec) with a calculated mechanical power to drive the legs of 0.51 mW.

INTRODUCTION

Microrobots (typically < 1 cm in length, < 100 mg in mass) that can move through real-world environments at insect-like speeds have potential application to search through small cracks in rubble after natural disasters or provide low-cost sensor deployment over civil infrastructure. However, multiple challenges in actuation, mechanism design, locomotion, integration, and power exist to engineer legged microrobots. This work focuses specifically on enabling fast locomotion in robots at these small scales.

The few microrobots (typically < 100 mg) that have walked have done so at slow speeds, less than 1 body length/sec. Hollar integrated solar cells and a CMOS controller with 50 µm thick, 1 mm long legs using polysilicon pin hinges to successfully demonstrate autonomous microrobot (l = 8.5 mm, m = 10 mg) motion, but not forward motion [1]. Ebefors demonstrated one of the more successful microrobots (l = 15 mm, m ~ 80 mg) that moved forward at speeds up to 6 mm/s and survived relatively rough handling, but required tethering due to the thermal actuators [2]. Also using tethered thermal actuators, Erdem demonstrated basic walking motion in a microfabricated robot (l = 3 cm, m = 0.5 g) [3].

At much larger scales, robots like iSprawl (l = 15 cm, m = 0.3 kg) and RHex (l = 0.5 m, m = 7 kg) have taken advantage of bio-inspired compliant leg designs to move at speeds of 10+ body lengths/sec [4], [5]. In between these size scales, robots like HAMR (l = 4.4 cm, m = 1.3 g) have demonstrated locomotion at speeds of 10 body length/sec in part due to the high power piezoelectric actuators used as well as the smart composite microstructures (SCM) enabling impressive 3D structures fabricated from an inherently 2D process [6].

Similar to iSprawl, this work takes advantage of a multi-material fabrication process described in [7] to create legs made from rigid silicon links with elastomer joints for compliance and robustness. Untethered high power actuation is achieved using an external magnetic field and embedded magnets in the robot, an approach used extensively by the fluidic microrobot community (e.g. [8]). The final microrobot tested in this work is shown in Fig. 1 (l = 4 mm, m = 25 mg).

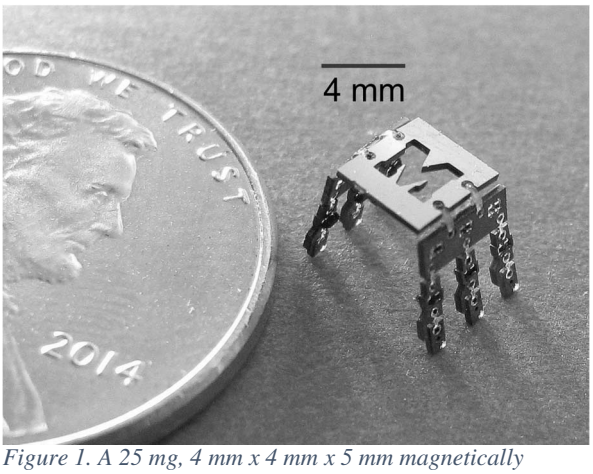

Figure 1. A 25 mg, 4 mm x 4 mm x 5 mm magnetically actuated walking microrobot

MICROROBOT DESIGN

Leg and Foot Design

The robot design was inspired by hexapedal insects, such as ants and cockroaches. The leg mechanism, pictured in Fig. 2 consists of two links and two joints, with a single point of actuation in the top link, resulting in a single active degree of freedom (DOF) in the hip joint and a single passive DOF in the knee joint. These joints are made from a softer material (i.e. silicone rubber), and can be modeled as a single torsion spring using the pseudo-rigid-body model, $k_\theta = \frac{EI}{l}$, where E is the modulus of the joint material, I is the second moment of area, and l is the length of the joint.

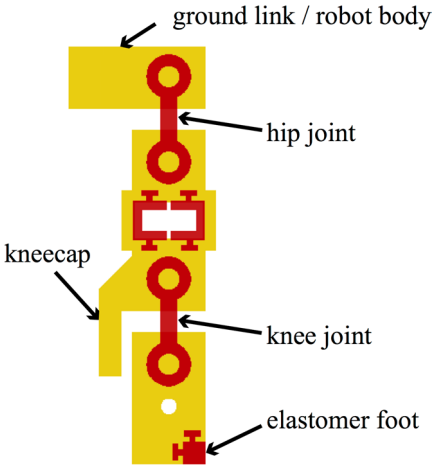

Figure 2. The leg design takes advantage of rigid (yellow = Silicon) and soft (red = elastomer) components to enable compliance. Asymmetry to enable forward locomotion in a symmetrically rotating magnetic field is provided through the kneecap and foot.

The actuation of the top link is symmetric, which would also generate symmetric leg motion and ultimately no forward progress in the robot. Therefore, asymmetries have been incorporated into the leg design: a hard mechanical stop on one side of the knee joint (a "kneecap") and a high-friction feature applied to only one side of the foot. The hard mechanical stop allows the knee joint to swing freely in one direction while stopping it to be in line with the upper link in the other, similar to [9], which drives the robot preferentially in the direction of the stop. The high-friction feature creates a differential friction in the foot, similar to [10], which drives the robot preferentially in the direction opposite to the high friction feature.

The dimensions for both of the joints are l = 200 µm x w = 100 µm x t = 300 µm, where t is the thickness of the leg. The dimensions of the top link are 1650 µm x 670 µm x 300 µm, and the dimensions of the bottom link are 1200 µm x 670 µm x 300 µm. The kneecap extends 600 µm from the bottom of the top length, with a resulting undeformed overlap of 400 µm between the kneecap and the lower link, with a gap of 100 µm separating the two. The foot feature measures 200 µm x 200 µm, and extends through the full 300 µm thickness of the leg.

The dimensions of this leg are not optimized, rather they were chosen to accommodate robust joint anchor geometry, and to not push the limits of the fabrication process in order to ensure good yield. A high-yield, robust design was chosen over a high-performance design to ensure that all six legs of a full hexapod are most likely to survive, as well as to ensure adequate test samples to characterize the performance of these legs to inform design choices on future iterations of leg design.

Magnetic Actuation

The robots in this paper are actuated by the interaction between permanent magnets embedded in the upper link of the robot legs (robot magnets) and the magnetic field generated by an external permanent magnet (actuator magnet). This approach results in untethered and high power actuation required to study locomotion at small scales without the need for integrated motors and power supplies. A point-dipole model is used to calculate the expected torque and force between two permanent magnets [11]. The field produced from the actuator magnet is given by

$$\boldsymbol{h} = \frac{1}{4\pi\|\boldsymbol{p}\|^3} H\boldsymbol{m_a}$$
$$H = 3\hat{\boldsymbol{p}}\hat{\boldsymbol{p}}^T - I \qquad (1)$$

where $\boldsymbol{p}$ is the vector describing the distance from the center of the actuator magnet to a point of interest and $\hat{\boldsymbol{p}}$ is the unit vector of $\boldsymbol{p}$. $\boldsymbol{m_a}$ is the three-dimensional vector of the magnetic dipole moment of the actuator magnet and I is the 3-by-3 identity matrix [11].

The robot magnets will attempt to align with the external field generated by the actuator magnet resulting in a torque on the robot magnets. The maximum available torque is given by

$$\|\tau\|_{max} = \mu_0 \|\boldsymbol{h}\| \|\boldsymbol{m_r}\| \qquad (2)$$

where μ_0 is the magnetic permeability, $\mu_0 = 4\pi \times 10^{-7}$ N/A^2 (in vacuum), $\boldsymbol{h}$ is the field calculated from Eqn. 1 and $\boldsymbol{m_r}$ is the magnetic dipole moment of the robot magnet embedded in the leg [11].

A force between the actuator magnet and robot magnets is also generated due to the magnetic field gradient generated by the actuator magnet. More detail on the magnitude of this force is provided in [12]. The experimental setup described below keeps this force vector pointing down (versus pulling the robot forward or backward) as much as possible.

FABRICATION

Microfabrication and Magnet Assembly

The microrobots are fabricated using the process described in Fig. 3. A through-wafer micro-molding process is used to create both high aspect ratio silicon and elastomer features for rigid parts of the robot and joints respectively. The wafer thickness in this work is 300 µm, and the process is similar to that described in [7] through step E.

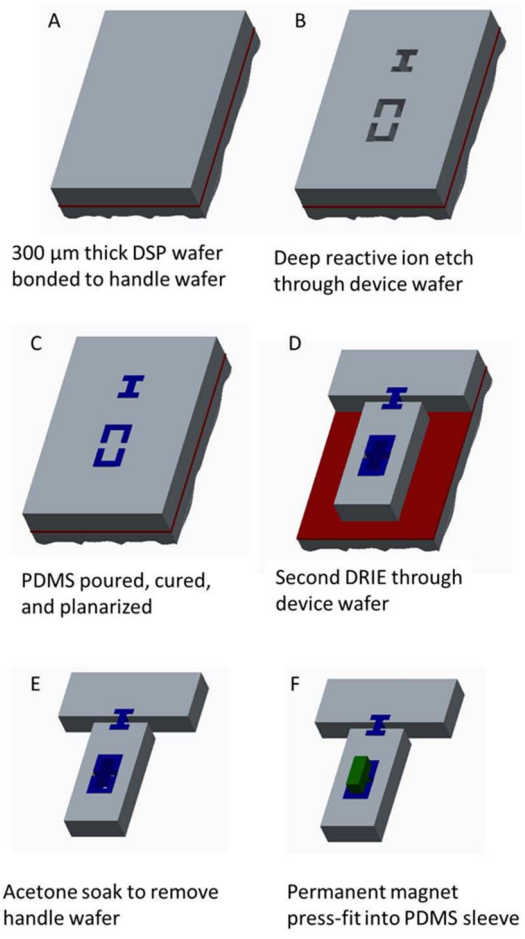

Figure 3. The fabrication process uses multiple DRIE steps to create both elastomeric features (C) and silicon features (E) in a through-wafer process. A commercially available magnet is embedded in an elastomer sleeve in (F).

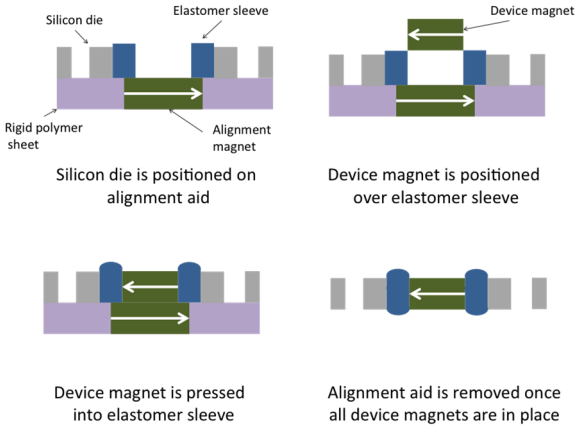

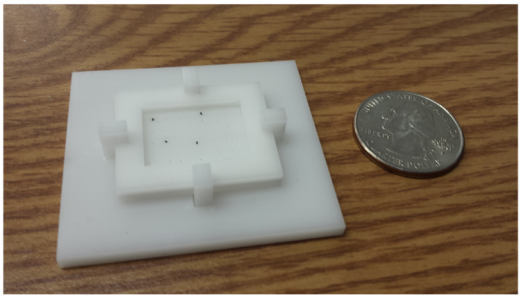

Figure 4. A schematic view of the magnet assembly process as well as the assembly jig used for the microrobots.

After release (in step F), a magnet alignment aid (Fig. 4) is used to help assemble 500 µm x 500 µm x 200 µm neodymium N50 magnets (SuperMagnetMan, S0050) in the robot with the proper orientation. The dipole of these magnets was experimentally measured as 34.6 µA-m^2. The orientation of the embedded robot magnets is defined to create a "tripod" gait in which the outer legs on one side of the robot and the middle leg on the other side operate synchronously. The magnet orientation on the other three legs is flipped 180°. This alignment aid is made from a laser patterned sheet of polymer that is populated with magnets in the proper orientation to encourage assembly. A thin laminate applied over the surface keeps the entire assembly in place.

Microrobot Assembly

Six of the legs described in the previous section were fabricated attached to a central body. The hexapod is fabricated in a planar, unfolded state, then is folded out-of-plane and the sides are held in place with a small amount of Loctite 409 gel superglue.

In order to aid in the out-of-plane assembly, small acrylic assembly pieces were laser cut with a defined sidewall angle, in this case 90°. The flat hexapods, already assembled with robot magnets in the legs, are put into the assembly pieces and held in place against the sidewalls using a small amount of water-soluble wax melted in place underneath the legs. A small amount of superglue is then placed between the robot body and the small slab of silicon where the legs are anchored on each side. The wax keeps the sides of the hexapod against the sidewalls and ensures that they are held at the defined sidewall angle while the glue is setting. Otherwise the glue will pull the sides of the hexapod in slightly during the curing process. The wax also provides a barrier between the hexapod and the assembly piece to prevent accidental affixing of the hexapod to the assembly piece. Once the glue is fully set, the water soluble wax is melted away with an overnight DI water soak. The final hexapod (Fig. 1) measures 4 mm x 4 mm x 5 mm, with a mass of 25 mg.

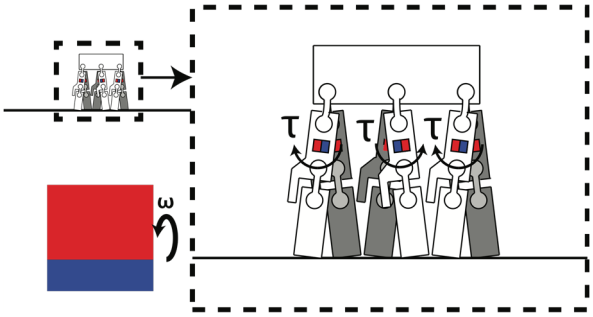

Figure 5. The experimental setup uses a rotating permanent magnet to generate the magnetic field that drives the robot legs. Magnets in the robot are assembled to drive the robot with a tripod gait.

EXPERIMENTAL RESULTS

Experimental Setup

Each hexapod was actuated by an external rotating magnetic field provided by mounting a 1 in^3 N55 neodymium magnet (the actuator magnet, with an experimentally measured dipole of 18.6 A-m^2) to a 25 mm diameter DC motor to generate a rotating magnetic field. The actuator magnet and motor were placed in brackets and attached to a linear stage (Zaber, A-LSQ450D-E01). A schematic view of the mounted magnet setup and its effect on the robot legs is shown in Fig. 5.

A thin sheet of acrylic is supported above the magnet. To maintain the desired separation distance between the actuator magnet and the robot, the magnet needs to be moved, keeping it centered under the hexapod. Since the microrobots were too small to use with an OptiTrack motion capture system (as used in [12]), a webcam was mounted above the hexapods to track the planar kinematic information of the robots. The measured velocity of the hexapod was sent to the stage to keep the magnet under it.

Each hexapod was tested walking on a flat acrylic sheet in this rotating magnetic field over at least 60 mm (corresponding to 15 body lengths). The longitudinal position was tracked to calculate robot speed at different motor frequencies (corresponding to different stride frequencies in the legs), and five trials were recorded at each speed. The position of the robot magnet dipoles relative to the actuator magnet dipole was set to 4.9 cm, corresponding to a maximum torque on each robot leg of 0.62 mN-mm and a downward force of 38 µN for each leg (corresponding to 90% of the robot's body weight for all six legs). This force acts as an additional load on the robot. Experiments in which the distance between the actuator magnet and robot was greater than 50.7 mm (corresponding to 3.2 body lengths or 3.2 body widths away from the position directly above the actuator magnet and a 10% decrease in available torque) at any point during the run were discarded.

Figure 7. Overlaid frames captured from video of the microrobot walking at approximately 1 body length/sec over 15 sec.

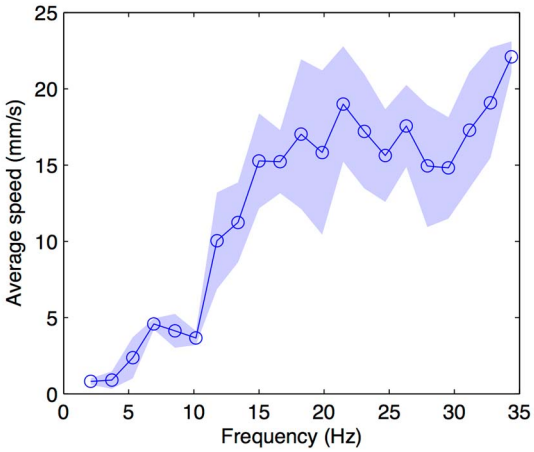

Figure 6. Speed results versus frequency of the rotating magnet (generally = microrobot stride frequency). The shaded area indicates the standard deviation over 5 trials and the circles represent the mean.

Locomotion Results

Screenshots from a typical locomotion trial are shown in Fig. 7. Results from a frequency sweep of the rotating magnet are provided in Fig. 6. Low frequencies resulted in low speeds but also small variation between trials. At 10-15 Hz, the locomotion clearly becomes more dynamic in nature, having an aerial phase. The standard deviation increases as this more dynamic motion also led to more deviation from a straight line in the robot's path. A maximum mean speed of 22.1 mm/sec was achieved, corresponding to 5.5 body lengths/sec. The maximum speed among all trials was found at 21.5 Hz and resulted in forward motion of the robot at 25.5 mm/sec and 6.4 body lengths/sec at a calculated power of 0.51 mW to drive the legs.

CONCLUSIONS

The fabrication, leg design and magnetic actuation described in this work has been used to engineer a dynamic, small and fast walking microrobot. The microrobot, even with a non-optimized leg design has shown significant speed improvements over previous walking microrobots at a similar scale, to walk at over 5 body lengths/sec. This work demonstrates that compliant legs and high power actuation with very simple control can still generate fast locomotion in small-scale robots. Future work using this approach will help improve understanding of low-mass robot locomotion, putting microrobots with dimensions and performance rivaling those of ants within our reach.

ACKNOWLEDGEMENTS

This work was supported by NSF PECASE Award ECCS1055675. We acknowledge the support of the Maryland NanoCenter and its FabLab.

REFERENCES

[1] S. Hollar, A. M. Flynn, C. Bellew, and K. S. J. Pister, "Solar powered 10 mg silicon robot," in *IEEE Micro Electro Mechanical Systems*, 2003, pp. 706–711.

[2] T. Ebefors, J. U. Mattsson, E. K"alvesten, and G. Stemme, "A Walking Silicon Micro-Robot," in *Transducers*, Sendai, Japan, 1999, pp. 1202–1205.

[3] E. Y. Erdem *et al.*, "Thermally Actuated Omnidirectional Walking Microrobot," *JMEMS*, vol. 19, no. 3, pp. 433–442, Jun. 2010.

[4] S. Kim, J. E. Clark, and M. R. Cutkosky, "iSprawl: Design and Tuning for High-speed Autonomous Open-loop Running," *IJRR*, vol. 25, no. 9, pp. 903–912, Sep. 2006.

[5] U. Saranli, M. Buehler, and D. E. Koditschek, "RHex: A Simple and Highly Mobile Hexapod Robot," *IJRR*, vol. 20, pp. 616–631, 2001.

[6] A. T. Baisch, O. Ozcan, B. Goldberg, D. Ithier, and R. J. Wood, "High speed locomotion for a quadrupedal microrobot," *IJRR*, vol. 33, no. 8, pp. 1063–1082, Jul. 2014.

[7] A. P. Gerratt and S. Bergbreiter, "Incorporating compliant elastomers for jumping locomotion in microrobots," *Smart Materials and Structures*, vol. 22, no. 1, p. 14010, Jan. 2013.

[8] E. Diller, "Micro-Scale Mobile Robotics," *Foundations and Trends in Robotics*, vol. 2, no. 3, pp. 143–259, 2011.

[9] J. E. Pratt and G. A. Pratt, "Exploiting natural dynamics in the control of a planar bipedal walking robot," in *Annual Allerton Conference on Communication, Control, and Computing*, University of Illinois, 1998, vol. 36, pp. 739–748.

[10] T. Senoo, M. Takano, and M. Ishikawa, "Dynamic horizontal movement of a bipedal robot using frictional asymmetry," in *IEEE/RSJ IROS*, Vilamoura-Algarve, Portugal, 2012, pp. 1834–1839.

[11] A. W. Mahoney and J. J. Abbott, "Generating Rotating Magnetic Fields With a Single Permanent Magnet for Propulsion of Untethered Magnetic Devices in a Lumen," *IEEE Transactions on Robotics*, vol. 30, no. 2, pp. 411–420, Apr. 2014.

[12] R. St. Pierre and S. Bergbreiter, "Gait exploration of sub-2 g robots using magnetic actuation," *IEEE Robotics and Automation Letters*, pp. 1–1, 2016.

CONTACT

*S. Bergbreiter, tel: 1-301-405-6506; sarahb@umd.edu